Energy transfer rates and population inversion investigation of $^1G_4$ and $^1D_2$ excited states of Tm^{3+} in Yb:Tm:Nd:KY_3F_{10} crystals

Horácio Marconi da Silva M. D. Linhares,[1] André Felipe Henriques Librantz,[2] Laércio Gomes,[1,a)] Lilia Coronato Courrol,[3] Sonia Lícia Baldochi,[1] and Izilda Marcia Ranieri[1]

[1]*Centro de Lasers e Aplicações, Instituto de Pesquisas Energéticas e Nucleares, IPEN-CNEN/SP, Butantã, P.O. Box 11049, São Paulo SP 05422-970, Brazil*

[2]*Departamento de Ciência Exatas, Universidade Nove de Julho, UNINOVE, São Paulo SP 02111-030, Brazil*

[3]*Departamento de Ciências Exatas e da Terra, Universidade Federal de São Paulo, UNIFESP, Diadema, São Paulo SP 09972-270, Brazil*

(Received 1 September 2010; accepted 4 January 2011; published online 22 April 2011)

In this work we present the spectroscopic properties of KY_3F_{10} (KY3F) single crystals activated with thulium and co-doped with ytterbium and neodymium ions. The most important processes that lead to the thulium up-conversion emissions in the blue and ultraviolet regions were identified. A time-resolved luminescence spectroscopy technique was employed to measure the luminescence decays and to determine the most important mechanisms involved in the up-conversion process that populates $^1G_4$ and $^1D_2$ (Tm^{3+}) excited states. Analysis of the energy-transfer processes dynamics using selective pulsed-laser excitations in Yb:Tm:Nd, Tm:Nd, and Tm:Yb KY3F crystals show that the energy transfer from Nd^{3+} to Yb^{3+} ions is the mechanism responsible for the enhancement of the blue up-conversion efficiency in the Yb:Tm:Nd:KY3F when compared with the Yb:Tm system. A study of the energy transfer processes in Yb:Tm:Nd:KY3F crystal showed that the $^1G_4$ excited level is mainly populated by a sequence of two nonradiative energy transfers that starts well after the Nd^{3+} and Tm^{3+} excitation at 797 nm according to: Nd^{3+} ($^4F_{3/2}$) → Yb^{3+} ($^2F_{7/2}$) followed by Yb^{3+} ($^2F_{5/2}$) → Tm ($^3H_4$) → Tm^{3+} ($^1G_4$). Results of numerical simulation of the rate equations system showed that a population inversion for 483.1 nm laser emission line is attained for a pumping rate threshold of 98 s^{-1}, which is equivalent to an intensity of 3.3 KW cm^{-2} for a continuous laser pumping at 797 nm for Yb(30 mol%):Tm(0.5 mol%):Nd(1 mol%):KY3F. Nevertheless, best Yb^{3+} concentration for the laser emission near 483.1 nm was estimated to be within 40 and 50 mol%. On the other hand, a population inversion was not observed for the case of 960 nm (Yb^{3+}) pumping. © *2011 American Institute of Physics*. [doi:10.1063/1.3552924]

I. INTRODUCTION

The study of solids doped with thulium ions has received great interest in the last decades due to the numerous applications of these materials. Concerning to the thulium emission wavelength, these solids can be used as laser materials[1] for different applications in life sciences,[2] light detection and ranging (LIDAR)[3] and industry or can be applied as the S-band Tm-doped fiber amplifier in wavelength-division-multiplexing telecommunication,[4] or for optical devices,[5] color displays,[6] and optical memories.[7] Due to the attractive thermo-mechanical properties, wide transparency and high optical damage threshold, KY3F has been studied as laser materials when activated by several RE^{3+} ions, which can easily substitute Y^{3+} ions in a noncenter-symmetrical site [C_{4v} symmetry].[8–12] KY3F has relatively low phonon energy (cutoff ~500 cm^{-1}) that is an important point in avoiding energy loss by nonradiative relaxation involving the $^1G_4$ and $^3H_4$ excited levels. KY3F is the only compound in the KF-YF_3 system that melts congruently without any phase transition. It crystallizes in the cubic fluorite-type structure (Fm3m) with a lattice parameter $a = 11.54$ Å,[12] which constitutes an isotropic crystal.

In this paper, KY_3F_{10} (KY3F) doped with thulium (Tm^{3+}) ions that are sensitized by neodymium (Nd^{3+}) and ytterbium (Yb^{3+}) were studied, and the multiples processes of energy transfer that occurs when this material is excited around 800 and near 960 nm were inspected and the transfer rates constants were determined. In light of potential directly diode pumped Tm^{3+}-doped KY3F:Yb:Nd crystal lasers, we numerically solved the rate equations for Yb(x):Tm(0.5 mol%):Nd(1 mol%):KY3F ($x = 5$, 10, 20, and 30 mol%) and Yb(20 mol%):Tm(0.5 mol%):KY3F under cw pumping at 797 nm to determine the population inversion and its dependence on the Nd^{3+} co-doping.

II. EXPERIMENTAL PROCEDURES

The rare earth fluorides were prepared from pure oxide powders (Alpha-Johnson Matthey, 99.99%) by hydrofluorination at high temperature in hydrofluoric acid (HF) atmosphere. The powder was contained in a cylindrical platinum boat, which was inserted in a sealed platinum tube. The KF-LnF_3 (Ln = Y, Yb, Nd, and Tm) mixture was melted using an open platinum boat in the same atmosphere, with a

a)Author to whom correspondence should be addressed. Electronic mail: lgomes@ipen.br.

composition of 1.02 KF: 1 LnF_3. KF powder (Alpha-Johnson Matthey, 99.9%) was zone-refined before it was added to the mixture. The KY3F samples were obtained in the same system by slow cooling. Mixtures of KF-LnF_3 were contained in a cylindrical platinum boat and melted around 990°C and cooled with a rate of ~10°C/h. The synthesized material had always-transparent crystalline regions from which the samples were extracted. The rare earths concentrations were obtained by inductively coupled plasma-optical emission spectroscopy (ICP-OES) analysis. The following crystals were grown and prepared for the luminescence measurements performed in this work: (i) Yb(5, 10, 20 and 30 mol%):Tm(0.5 mol%): Nd(1 mol%): KY3F, (ii) Yb(5, 10 and 20 mol%): Tm(0.5 mol%):KY3F, and (iii) Tm(0.5 mol%): Nd(1 mol%):KY3F.

The absorption spectra of all samples were measured in the range 700−2500 nm at room temperature using a Varian Cary 17D/OLIS spectrophotometer. In the luminescence lifetime measurements, the samples were excited by pulsed laser radiation generated by a tunable OPO-IR pumped (Rainbow from OPOTEK, USA) by the second harmonic of a Q-switched Nd:YAG (yttrium aluminum garnet) laser (Brilliant B from Quantel, France). Laser pulse widths of 4 ns at 960 and 797 nm were used to directly excite the $^2F_{5/2}$ and $^3H_4$ excited states of Yb^{3+} and Tm^{3+}, respectively. Luminescence signals were analyzed by the 0.25 m Kratos monochromator, detected by the EMI S-20 (or S-1) photomultiplier tube (PMT) (response time of 10 ns) or InSb 77 K infrared detector from Judson (response time ~0.5 μs) and resolved by the EGG Boxcar Processor model 4402 computer interfaced by the general purpose interface bus (GPIB) port. Luminescence lifetime was measured using a digital oscilloscope of 100 MS s^{-1} model TDS 410 from TEKTRONIX interfaced to a microcomputer.

III. EXPERIMENTAL RESULTS

Optical absorption spectra of KY3F doped Yb:Tm:Nd crystal has two main absorptions in the near infrared around 960 nm (Yb^{3+}) and around 800 nm due to Nd^{3+} and Tm^{3+} ions. The most intense absorption is near 960 nm due to high concentration of ytterbium in the samples (10%) as seen in Fig. 1. When KY3F crystal containing Tm^{3+} co-doped with Yb^{3+} or Yb^{3+} and Nd^{3+} is excited at 797 nm, blue 470–480 nm Tm^{3+}-emission is observed and the blue emission strongly increases for neodymium co-doping with 1 mol%, see the results shown in Fig. 2. These luminescence effect is similar to one reported for YLF crystal were it has been demonstrated that Yb(20 mol%):Tm(0.5 mol%) co-doped with Nd^{3+} (~1 mol%) causes an accentuated enhancement of the Tm^{3+} blue emission indicating that Nd^{3+} ions significantly contribute to the population of the $^1G_4$ excited level that emits around 480 nm (Ref. 13). As a minor effect, the population of the $^1G_4$ excited level may interacts with $^2F_{5/2}$ (Yb^{3+}) exciting the $^1D_2$ (Tm^{3+}) level, which emits near 360 and 450 nm. Figure 3 shows the schematic energy diagram levels of Yb/Tm/Nd system. The most of indicated processes will be discussed and proved to be essential for the blue emission up-conversion by the luminescence dynamics analysis in the sequence. When the Yb:Tm:Nd or Tm:Nd samples are excited at 792–797 nm the following processes are observed to occur:

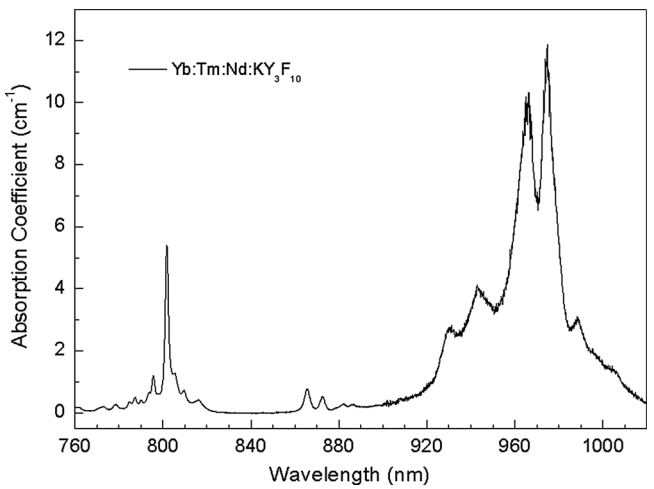

FIG. 1. Absorption spectrum of Yb(10 mol%):Tm(0.5 mol%):Nd(1 mol%): KY3F crystal in the near infrared measured at T = 300 K.

(*a*) Ground state absorption of Nd^{3+} ($^4I_{9/2}$) → Nd^{3+} ($^4F_{5/2}$),
(*a′*) Ground state absorption of Tm^{3+} ($^3H_6$) → Tm^{3+} ($^3H_4$),
(*b*) Nd–Yb energy transfer
Nd ($^4F_{3/2}$) + Yb ($^2F_{7/2}$) → Nd ($^4I_{11/2}$) + Yb ($^2F_{5/2}$),
(*c*) Nd–Tm energy transfer
Nd ($^4F_{3/2}$) + Tm ($^3H_6$) → Nd ($^4I_{15/2}$) + Tm ($^3F_4$),
(*d*) Tm–Yb back-transfer
Tm ($^3H_4$) + Yb ($^2F_{7/2}$) → Tm ($^3H_6$) + Yb($^2F_{5/2}$),
(*e*) Yb × Tm cross-relaxation
Yb($^2F_{5/2}$) + Tm ($^3H_6$) → Yb ($^2F_{7/2}$) + Tm ($^3H_5$),
(*f*) Yb × Tm cross-relaxation
Yb ($^2F_{5/2}$) + Tm ($^3F_4$) → Yb ($^2F_{7/2}$) + Tm ($^3H_4$),
(*g*) Yb × Tm cross-relaxation
Yb($^2F_{5/2}$) + Tm ($^3H_4$) → Yb ($^2F_{7/2}$) + Tm ($^1G_4$),
(*h*) Yb × Tm cross-relaxation
Yb($^2F_{5/2}$) + Tm ($^1G_4$) → Yb ($^2F_{7/2}$) + Tm ($^1D_2$),
(*i*) Nd × Tm cross-relaxation
Nd($^4F_{3/2}$) + Tm ($^3H_4$) → Nd ($^4I_{11/2}$) + Tm ($^1G_4$),
(*p*) Tm − Nd energy transfer
Tm ($^3F_4$) + Nd ($^4I_{9/2}$) → Tm ($^3H_6$) + Nd ($^4I_{15/2}$),
(*q*) Tm−Nd energy transfer
Tm ($^3H_4$) + Nd ($^4I_{9/2}$) → Tm ($^3H_6$) + Nd ($^4F_{5/2}$),
(*r*) Tm × Tm cross-relaxation
Tm ($^3H_4$) + Tm ($^3H_6$)→ Tm ($^3H_5$) + Tm ($^3F_4$),
(*s*) Tm × Tm cross-relaxation
Tm ($^1G_4$) + Tm ($^3H_6$)→ Tm ($^3H_5$) + Tm ($^3H_4$).

The luminescence transient of an acceptor state that is indirectly excited by the donor-acceptor (or D-A) energy transfer is given by Eq. (1), which has been derived elsewhere[14] for an energy transfer that includes Burshtein (or Inokuti-Hirayama, where $\omega = 0$) model due to a dipole-dipole interaction.

$$I_1(t) = I_0\left\{\exp\left(-\frac{t}{\tau_A}\right) - \exp\left(-\frac{t}{\tau_d} - \omega t - \gamma\sqrt{t}\right)\right\}, \quad (1)$$

where τ_A is the total lifetime of the acceptor (A) excited state and τ_d is the intrinsic lifetime of the donor (D) excited ion.

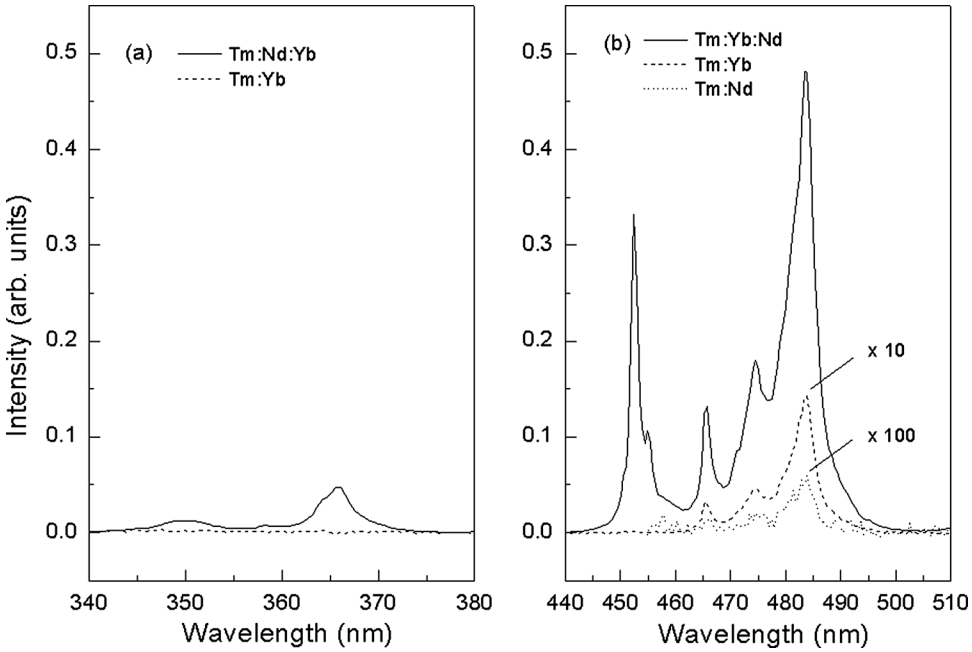

FIG. 2. shows the $^1D_2 \rightarrow {}^3H_6$ emission (Tm^{3+}) around 365 nm (a) and the $^1D_2 \rightarrow {}^3F_4$ and $^1G_4 \rightarrow {}^3H_6$ emissions of Tm^{3+} near 450 and 480 nm, respectively, for the Yb(20):Tm(0.5):Nd(1):KY3F, Yb(20):Tm(0.5):KY3F, and Tm(0.5):Nd(1):KY3F crystals under cw laser pumping at 797 nm (T = 300 K).

The first term of Eq. (1) gives the luminescence decay of the acceptor and the second gives the luminescence rise time, which should be equal to the donor total lifetime. The rise time constant was obtained by integration according to Eq. (2) for the case of nonexponential process.

$$\tau = \int_0^\infty \exp\left(-\frac{t}{\tau_d} - \omega t - \gamma\sqrt{t}\right) dt. \qquad (2)$$

For instance, if the diffusion process between donor states dominates the energy transfer mechanism (or $\omega \gg \gamma^2$) the donor decay will be exponential and the acceptor rise time will be exponential. That is the case observed of all the Yb → Tm transfers in Yb:Tm:Nd and Yb:Tm systems observed in this paper because of the high Yb^{3+} concentration used (> 5 mol%). In this case, the acceptor luminescence fitting was performed using Eq. (3).

$$I_2(t) = I_0\left\{\exp\left(-\frac{t}{\tau_A}\right) - \exp\left(-\frac{t}{\tau_D}\right)\right\} \text{ when } \tau_A > \tau_D \text{ or}$$
$$I_2'(t) = I_0\left\{\exp\left(-\frac{t}{\tau_D}\right) - \exp\left(-\frac{t}{\tau_A}\right)\right\} \text{ if } \tau_A < \tau_D. \qquad (3)$$

A. Nd−Yb energy transfer

Figure 4(a) shows the $^2F_{5/2}$ up-conversion luminescence transient of Yb^{3+} measured at 1000 nm for Yb(20%):Tm(0.5%):Nd(1%):KY3F after pulsed laser excitation at 868 nm with 4 ns of pulse duration. Best fit of Yb^{3+} luminescence transient (1000 nm) was performed using Eq. (3) and $\tau_{rise(2)} = 0.25$ μs and $\tau_{decay(2)} = 705$ μs were obtained from best fitting using a least squares fit with a correlation coefficient equal to 0.988. For instance, the transfer rate of process *b* was obtained using the relation $b = 1/\tau_{rise(2)}\text{-}1/\tau_{d9}$ that gave

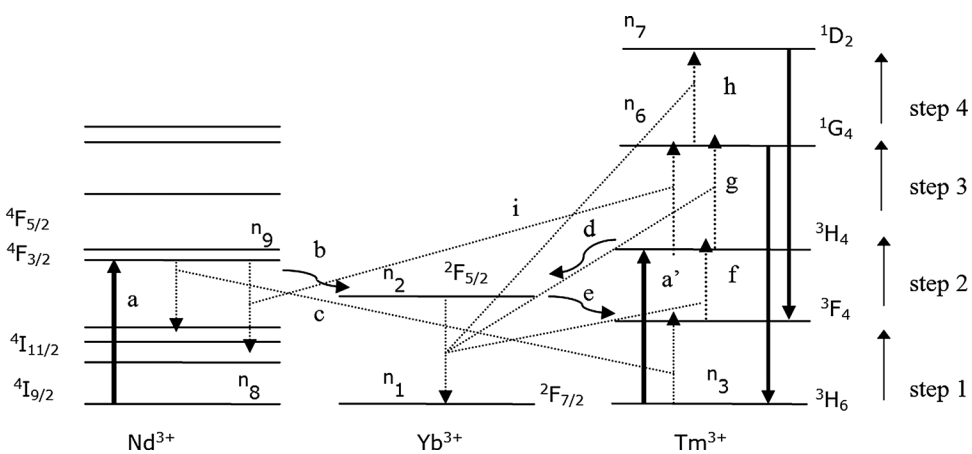

FIG. 3. Energy levels scheme and energy transfer mechanisms of Yb:Tm:Nd system. Solid line (up) 797 nm excitation. Solid lines (down) Tm^{3+} emissions (450 and 480 nm). Dot lines (up and down) Yb^{3+} emission and cross relaxation processes.

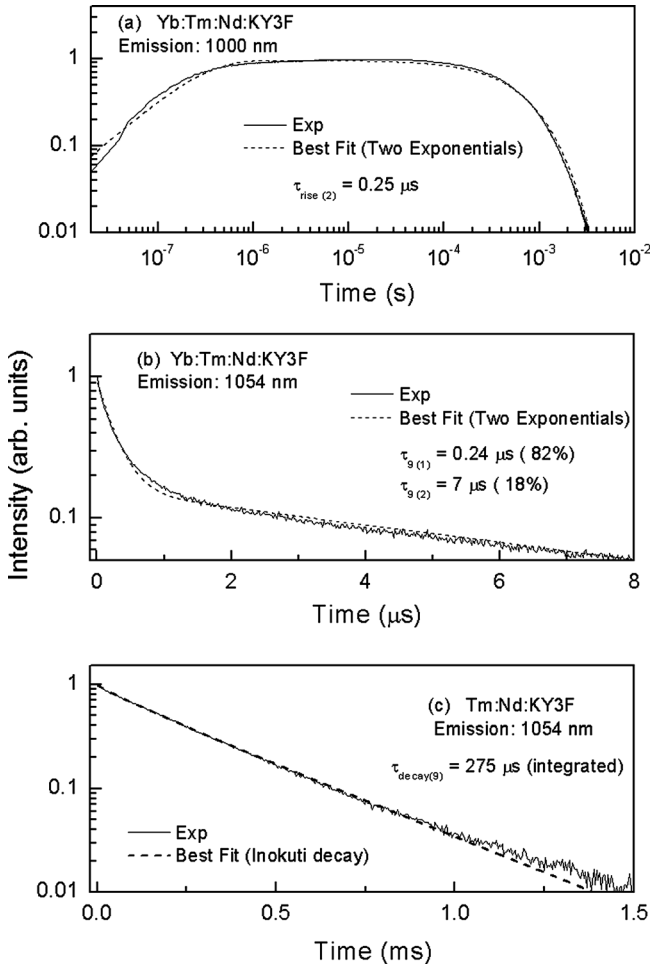

FIG. 4. (a) shows the luminescence transient of $^2F_{5/2}$ (Yb^{3+}) excited state measured at 1000 nm after pulsed laser excitation at 868 nm for Yb(20):Tm(0.5):Nd(1):KY3F. (b) and (c) show the luminescence decay of $^4F_{3/2}$ (Nd^{3+}) level directly excited by pulsed laser excitation at 868 nm for Yb(20):Tm(0.5):Nd(1) and Tm(0.5):Nd(1), respectively. Plots were made in double logarithmic scales for better show the model fitting used (solid lines represent the experimental measurements and dashed lines represent the best fittings). A correlation coefficients equal to 0.988, 0.997, and 0.999 were obtained from best fittings shown in (a), (b), and (c), respectively.

the rate constant b equals to 4×10^6 s^{-1} were $\tau_{d9} = \tau_d = 345$ μs (from the best fit). Figure 4(b) and 4(c) show the luminescence decay of $^4F_{3/2}$ (Nd^{3+}) measured at 1054 nm for Yb(20%):Tm(0.5%):Nd(1%) system and Tm(0.5%):Nd(1%) systems, respectively. A fast decay of $^4F_{3/2}$ (Nd^{3+}) luminescence at 1054 nm was observed for Yb:Tm:Nd system having two components decay of $\tau_{decay} = 0.24$ μs (82%) and $\tau_{decay} = 7$ μs (18%). Best fit o luminescence decay of Nd^{3+} in Tm:Nd system were obtained using Eq. (1) having $\gamma = 16.05$ $s^{-1/2}$ and $\tau_d = 345$ μs where $\omega \sim 0$ and $R^2 = 0.999$. The $^4F_{3/2}$ (Nd^{3+}) lifetime was obtained using Eq. (2) that gave $\tau = \tau_9 = 275$ μs for Tm:Nd system. This result clearly shows that the energy transfer $Nd(^4F_{3/2}) + Tm(^4H_6) \rightarrow Nd(^4I_{15/2}) + Tm(^3F_4)$ (process c) observed to occur in Tm:Nd system, should be negligible for Yb:Tm:Nd system because the time constant involved in the $Nd(^4F_{3/2}) \rightarrow Yb(^2F_{7/2})$ transfer (0.25 μs) is much shorter than the one involved in the $Nd(^4F_{3/2}) \rightarrow Tm(^3H_6)$ transfer (275 μs). Nevertheless, the transfer rate of process c was obtained using the relation $c = 1/\tau_9 - 1/\tau_{d9}$ that gave the rate constant c equals to 738 s^{-1} were $\tau_{d9} = \tau_d = 345$ μs (from the best fit).

B. Yb–Tm interaction (step 1)

Figure 5(a) shows the $^3F_4$ luminescence transient of Tm^{3+} measured at 1900 nm for Yb(20%):Tm(0.5%):Nd(1%):KY3F after the pulsed laser excitation of Yb^{3+} ions at 960 nm ($E = 10$ mJ). Best fit of Tm^{3+} luminescence transient (1900 nm) was performed using Eq. (3) and $\tau_A = \tau_4 = 1.9$ ms and $\tau_D = \tau_{rise} = 388$ μs are the derived time constants using a least squares fit with a correlation coefficient equals to 0.998. The transfer rate constant of process e was obtained using the relation $e = 1/\tau_{rise} - 1/\tau_{d2}$, where $\tau_{rise} = 388$ μs and $\tau_{d2} = 3.5$ ms (lifetime of $^2F_{5/2}$ state of Yb^{3+} measured for the Yb(10%):KY3F crystal). One gets $e = 2291$ s^{-1}. The transfer rate constant of process p was obtained using the relation $p = 1/\tau_4 - 1/\tau_{d4}$, where $\tau_4 = 1.9$ ms and $\tau_{d4} = 9.4$ ms (the intrinsic lifetime of $^3F_4$ level[15]). One gets $p = 420$ s^{-1}.

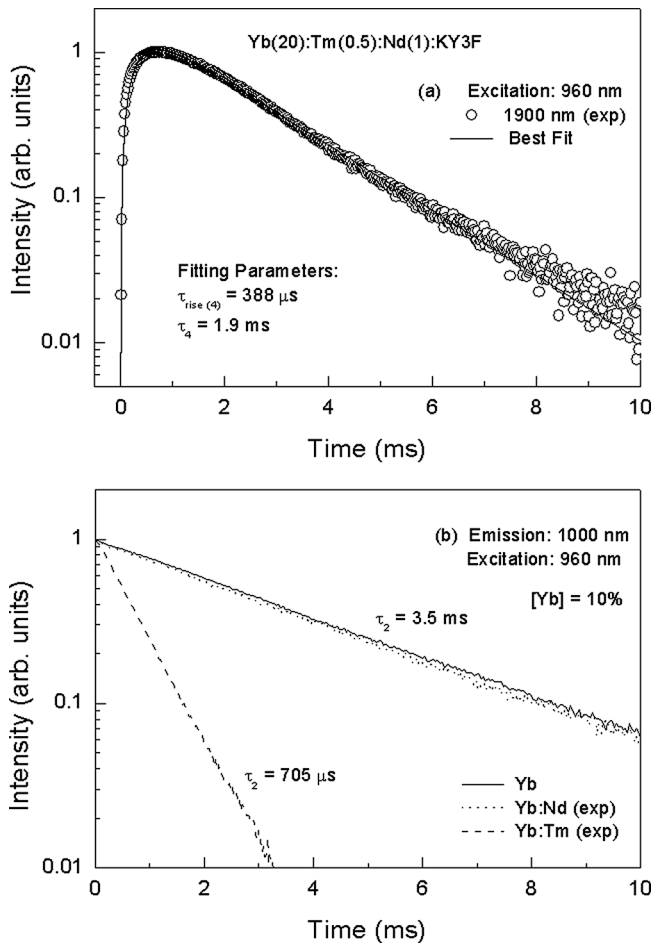

FIG. 5. (a) shows the luminescence transient of $^3F_4$ (Tm^{3+}) excited state measured at 1900 nm after pulsed laser excitation at 960 nm for Yb(20):Tm(0.5):Nd(1):KY3F (circles are representing the experimental data). Plot was made in logarithmic scale of decay for better show the model fitting used. A correlation coefficient equal to 0.998 was obtained for the best fitting represented by the solid line). (b) Shows the luminescence decay of Yb^{3+} measured at 1000 nm after the pulsed laser excitation at 960 nm for three systems: Yb(10):KY3F, Yb(10):Nd(1):KY3F, which show $\tau_2 = 3.5$ ms and Yb(10):Tm(0.5):KY3F with $\tau_2 = 750$ μs.

Figure 5(b) shows the luminescence decay of Yb(10%), Yb(10%):Nd(1%) and Yb(10%):Tm(0.5%) measured at 1000 nm after a pulsed laser excitation at 960 nm. Best fittings were done using an exponential decay, which shows that the $^2F_{5/2}$ level lifetime of Yb^{3+} in Yb(10):KY3F crystal ($\tau_2 = 3.5$ ms) is longer than the expected lifetime $\tau_{d2} = 1.8$ ms[15] due to the excitation migration contribution. Also, we see $\tau_2 = 3.5$ ms for Yb(10%):Nd(1%) system, which shows that there is no excitation transfer from Yb($^2F_{5/2}$) to Nd($^4F_{3/2}$) ions (or back transfer) in KY3F crystal. Figure 5(b) also shows the lifetime of Yb($^2F_{5/2}$) excited state decreases to 705 μs in Yb(20%):Tm(0.5%) due to the Yb → Tm energy transfer (process *e*). It was expected that τ_2 equals 390 μs according to the result of Fig. 5(a). However, one must to consider that not all the excited Yb^{3+} ions will interact with Tm^{3+} ions in Yb(20):Tm(0.5)-doped system and a fraction of isolated Yb^{3+} excited ions will remain. By this argument, one can consider that the $^2F_{5/2}$ (Yb^{3+}) luminescence exhibited in Fig. 5(b) should be composed of two components: (i) one due to the partial isolated Yb^{3+} ions emission with a lifetime of 3.5 ms (51%) and (ii) due to the (Yb−Tm) ions with a lifetime of 390 μs (49%). This gives a mean lifetime equal to 705 μs for the $^2F_{5/2}$ excited level of Yb^{3+}.

C. Yb−Tm interaction transfer (step 2)

The $^3H_4$ luminescence transients of Tm^{3+} observed at 800 nm were measured after pulsed laser excitations at 960 and 783 nm are shown in Figs. 6(a) and 6(b), respectively. Pulsed laser excitation at 960 nm ($E \sim 10$ mJ) was used to excite the $^3H_4$ (Tm^{3+}) up-conversion luminescence at 800 nm for Yb(20%):Tm(0.5%):Nd(1%) system as seen in Fig. 6(a). Best fit of Tm^{3+} luminescence transient (800 nm) was performed using $I_{2'}(t)$ expression given by Eq. (3) (for the case where $\tau_A < \tau_D$) from where best fitting parameters $\tau_A = \tau_{rise(5)} = 200$ μs and $\tau_D = \tau_5 = 563$ μs are the derived parameters using a least squares fit with a correlation coefficient equals to 0.995. One may observe that the $^3H_4$ luminescence rise time (~200 μs) is longer than the lifetime of $^3H_4$ excited state (τ_5) measured for the Yb(20%):Tm(0.5%):Nd(1%) system, which is equals to 145 μs [see Fig. 6(b)]. However, one must to consider the time transient of a composed donor obtained by the cross product of $^2F_{5/2}$ (Yb^{3+}) luminescence decay (level 2) and the $^3F_4$ (Tm^{3+}) luminescence transient (level 4), which gives the donor rise time, $\tau_{rise(24)}^{(donor)} = \left[(1/\tau_2) + (1/\tau_{rise(4)})\right]^{-1}$ for the case of $^2F_{5/2}$ (Yb^{3+}) excitation (~960 nm) once the decay and rise times are taken exponentials. Using $\tau_2 = 705$ μs and $\tau_{rise(4)} = 388$ μs one gets $\tau_{rise(24)}^{(donor)} = 250$ μs. The energy transfer rate of *process f* can now be calculated using the relation $f = 1/\tau_{rise(5)} - 1/\tau_{rise(24)}^{(donor)} \approx 1000$ s^{-1}. By the same argument, one can get $\tau_{decay(24)}^{(donor)} = [(1/\tau_2) + (1/\tau_4)]^{-1}$. Using $\tau_2 = 705$ μs and $\tau_4 = 1.9$ ms (both measured in this work) we get $\tau_{decay(24)}^{(donor)} = 514$ μs that is very consistent with the experimental value $\tau_5 = 570$ μs obtained from best fitting in Fig. 6(a).

Best fit of the $^3H_4$ luminescence decay for the Yb(20%):Tm(0.5%) system was done using the second term of Eq. (1) were $\gamma = 19$ $s^{-1/2}$ and $\omega = 0$ and $\tau_{d5} = 0.95$ ms are the derived parameters from the fitting of the experimental data (open circles) [solid line of Fig. 6(b)]. A decay time of $\tau_{decay(5)}^{(integrated)} = 600$ μs was obtained using Eq. (2). The transfer rate of process *d* could be calculated using the relation $d = 1/\tau_{decay(5)}^{(integrated)} - 1/\tau_{d5}$, which gives $d = 580$ s^{-1}. Results presented in Fig. 6(b) show that the $^3H_4$ (Tm^{3+}) excited level is strongly deactivated by Nd^{3+} ions for the Yb:Tm:Nd system (process *q*) similar to the case of Tm:Nd system. Best fit of the $^3H_4$ luminescence decay for the Tm:Nd system was done using the second term of Eq. (1) where $\gamma = 100$ $s^{-1/2}$ and $\omega = 0$ and $\tau_{d5} = 1.2$ ms are the derived parameters from the fitting of the experimental data (open triangles) [solid line of Fig. 6(b)]. A decay time of $\tau_{decay(5)}^{(integrated)} = 145$ μs was obtained using Eq. (2). The rate constant of process *q* was calculated using the relation $q = 1/\tau_{decay(5)}^{(integrated)} - 1/\tau_{d5}$, which gives $q = 6063$ s^{-1}. $Tm(^3H_4):Tm(^3H_6)$ cross-relaxation rate (process *r*) was estimated to be negligible in the case of KY3F crystal single

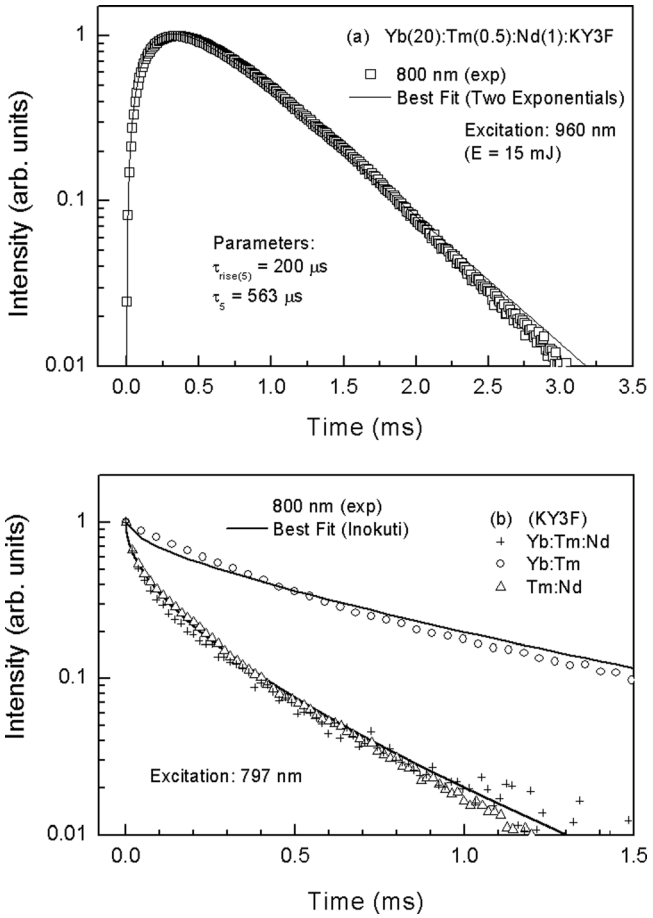

FIG. 6. (a) Shows the luminescence transient of $^3H_4$ (Tm^{3+}) excited state measured at 800 nm after pulsed laser excitation at 960 nm ($E \sim 15$ mJ) for Yb(20):Tm(0.5):Nd(1):KY3F (experimental data are represented by open squares) and the best fit with a correlation coefficient equals to 0.995 (solid line). (b) Shows the luminescence decays of $^3H_4$ (Tm^{3+}) level directly excited by pulsed laser excitation at 797 nm (E~8 mJ) measured for Yb(20):Tm(0.5):Nd(1) (crosses), Yb(20):Tm(0.5) (open circles) and Tm(0.5%):Nd(1%) (open triangles) KY3F crystals. Plots were made in a logarithmic scale to better show the model fit used (solid lines). The correlation coefficients for the fittings shown in (b) were 0.998 and 0.993 for the Yb:Tm and Tm:Nd systems.

doped with 0.5 mol% of thulium because we have verified that the decay time of $^3H_4$ excited state of Tm^{3+} that is equals to 1.2 ms is very close to the radiative lifetime value of 1.14 ms.[15]

D. Yb−Tm interaction (step 3)

The luminescence transient of $^1G_4$ level of Tm^{3+} measured at 480 nm after laser 798 nm laser pulsed excitation (E = 13 mJ) is showed in the Fig. 7(a). Best fit of $^1G_4$ luminescence transient was performed using $I_2(t)$ expression given by Eq. (3) (for the case where $\tau_A > \tau_D$) from where best fitting parameters $\tau_D = \tau_{rise(6)} = 230$ μs and $\tau_A = \tau_6 = 480$ μs are the derived parameters using a least squares fit with a correlation coefficient equals to 0.989.

It is noticeable that the $^1G_4$ up-conversion luminescence is generated at expenses of a cross interaction between $^2F_{7/2}$ (Yb^{3+}) (level 2) and $^3H_4$ (Tm^{3+}) (level 5) excited levels directly excited by 798 nm pulsed laser excitation. A time transient of the composed donor is obtained by the cross product of $^2F_{5/2}$ (Yb^{3+}) luminescence decay (level 2) and the $^3H_4$ (Tm^{3+}) luminescence decay (level 5), which gives

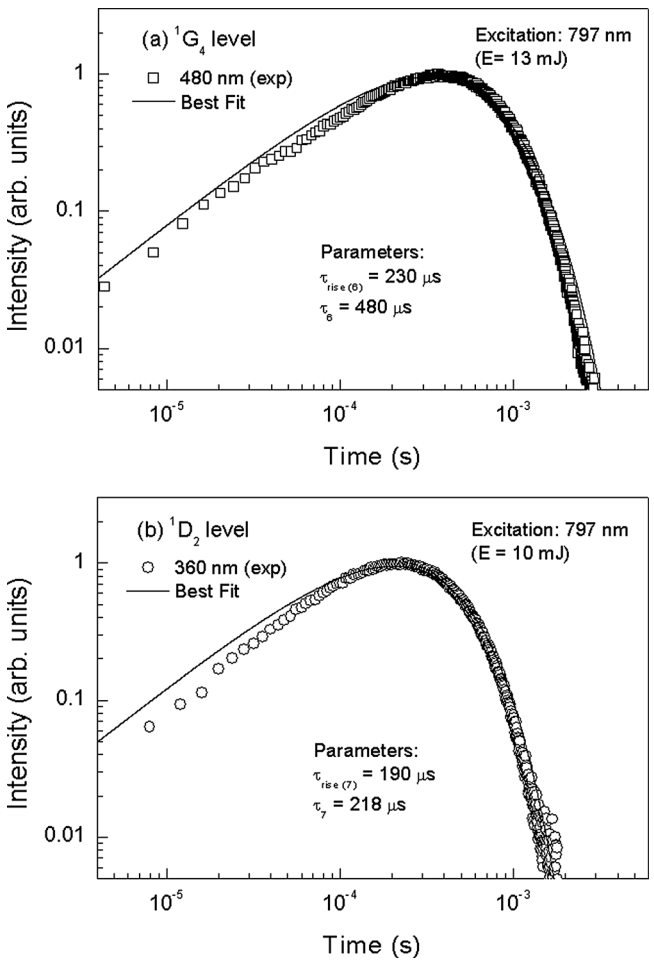

FIG. 7. Decay time of the luminescence transients of $^1G_4$ and $^1D_2$ levels of Tm^{3+} excited by pulsed laser at 797 nm in Yb(20):Tm(0.5):Nd(1):KY3F crystal. $^1G_4$ and $^1D_2$ excited states were measured by observing the time dependence of the 480 nm (a) and 360 nm (b) emissions, respectively. Solid lines represent the best luminescence fittings with a correlation coefficients: 0.989 and 0.993, respectively.

the composed donor decay time constant, $\tau^{(donor)}_{decay(25)} = [(1/\tau_2) + (1/\tau_5)]^{-1}$ for the Yb:Tm:Nd system. However, two distinct values of composed donors decay constants are obtained and need to be considered. A short decay for the composed donor, $\tau^{(donor)}_{decay(25)} = 120$ μs is obtained by considering that the decay time of $^3H_4$ level is dominated by the Tm−Nd interaction where $\tau_5 = 145$ μs was measured for Tm:Nd system. In this case, $\tau_{rise(6)} < \tau^{(donor)}_{decay(25)}$ what makes this process unavailable.

On the other hand, if one uses the decay time constant of $^3H_4$ (Tm^{3+}) measured for Yb(20%):Tm(0.5%) system ($\tau_5 = 600$ μs) one gets $\tau^{(donor)}_{decay(25)} \sim 324$ μs, which is longer than the measured rise time of $^1G_4$ luminescence transient (~230 μs). An assumption is made here that most of the Tm^{3+} excited ions rapidly migrates through $^3H_4$ excited states until get trapped by $Tm^{3+}(^3H_4)$ x $Yb^{3+}(^2F_{5/2})$ cross interaction such that the effective lifetime of $^3H_4$ (Tm^{3+}) level in Yb(20):Tm:Nd should be equal to the one verified for Yb(20%):Tm(0.5%) system (~600 μs). The transfer rate constant of process g was obtained from relation $g = 1/\tau_{rise(6)} - 1/\tau^{(donor)}_{decay(25)}$ where $\tau_{rise(6)} = 230$ μs and $\tau^{(donor)}_{decay(25)} = 324$ μs, which gave $g = 1260\ s^{-1}$.

$Tm(^1G_4):Tm(^3H_6)$ cross-relaxation rate (process s) was calculated using the decay constant of $^1G_4$ level measured for Yb:Tm:Nd system, where $s = 1/\tau_6 - 1/\tau_{R6}$. Using $\tau_6 = 480$ μs and the radiative lifetime of $^1G_4$ (Tm^{3+}) excited state equals to $\tau_{R6} = 649$ μs[15] we get $s = 543\ s^{-1}$.

E. Yb–Tm interaction (step 4)

The luminescence transient of $^1D_2$ level of Tm^{3+} measured at 360 nm after pulsed laser excitation at 798 nm (E = 10 mJ) is showed in the Fig. 7(b). Best fit of $^1D_2$ luminescence transient was performed using $I_2(t)$ expression given by Eq. (3) (for the case where $\tau_A > \tau_D$) from where best fitting parameters $\tau_D = \tau_{rise(7)} = 190$ μs and $\tau_A = \tau_7 = 218$ μs are the derived parameters using a least squares fit with a correlation coefficient equals to 0.993. One must to note that the $^1D_2$ up-conversion luminescence is generated at expenses of a cross interaction between $^2F_{7/2}$ (Yb^{3+}) (level 2) and $^1G_4$ (Tm^{3+}) (level 6) excited states by 797 nm pulsed laser excitation giving the following rise time and decay constant for Yb:Tm:Nd system:

$$\tau^{(donor)}_{rise(26)} = \left[\frac{1}{\tau_2} + \frac{1}{\tau_{rise(6)}}\right]^{-1} \quad \text{and} \quad \tau^{(donor)}_{decay(26)} = \left[\frac{1}{\tau_2} + \frac{1}{\tau_6}\right]^{-1}.$$

The donor composed transient has the following calculated rise and decay constants: $\tau^{(donor)}_{rise(26)} = 173$ μs and $\tau^{(donor)}_{decay(26)} = 286$ μs for Yb(20%):Tm(0.5%):Nd(1%) system. One must to note that the rise time constant measured for the $^1D_2$ level equals to 190 μs is slightly longer than the calculated one from the donor composed transient (173 μs) and therefore it should not contains the energy transfer rate process (h) we are looking for. Nevertheless, the measured decay time constant of $^1D_2$ state equal to 218 μs is much shorter than the calculated value of the donor composed transient equal to 286 μs, allowing to obtain the transfer

parameter h (rate) using the relation $h = 1/\tau_7 - 1/\tau_{decay(26)}^{(donor)}$, which gives $h = 1090\ s^{-1}$

F. Model for Yb – Tm interaction involving two ions in the excited state

A detailed investigation of the time dependence of the $^1D_2$ and $^1G_4$ up-conversion luminescence transients (step 3 and 4) was carried out by monitoring the up converted luminescence at 360 and 480 nm as a function of the absorbed excitation energy density by Tm^{3+} ions (N^*). We made a fit to the luminescence transient using two exponentials, $I_2(t)$. The rate parameters were obtained in the same way as described in Sec. III D. The result is presented in Table I. Figure 8 exhibits the rate probabilities g [Fig. 8(a)] and h [Fig. 8(b)] as a function of the density of excited Tm^{3+} ions. It can be observed that the rate parameter of process g reaches a constant rate when the excited Tm^{3+} ion density reaches a value of $8 \times 10^{18}\ cm^{-3}$, while the rate probability h reaches a constant value for $N^* \sim 5 \times 10^{18}\ cm^{-3}$-see Fig. 8(b). This behavior suggests the existence of a critical distance R_C between a Tm^{3+} excited ion and an Yb^{3+} indirectly excited by $Nd \rightarrow Yb$ transfer with a time constant of 0.25 μs, comprising the Yb−Tm cross relaxation, process g in this work. Based on the statistically random separation between the excited Yb^{3+} and Tm^{3+} ions in the crystal lattice, we say that the transfer efficiency of process g and h as a function of N^* is given by[16,17]

$$\eta = 1 - \exp(-N^*/N_C), \tag{4}$$

where N^* is the concentration of Tm^{3+} excited ions (cm^{-3}) and N_C is the critical concentration of excited Tm^{3+} ions which is related to the critical radius R_C. The observation that Yb–Tm rate parameter dependence on N^* in Figs. 8(a) and 8(b) display a constant probability rate for higher excitation densities indicates that the Yb-Tm relative efficiency for

TABLE I. Parameters used in the rate equation modeling for Yb(20%):Tm(0.5%):Nd(1%):KY_3F_{10} crystal.

Luminescence branching ratio and radiative lifetimes of Tm^{3+}[a]

Transition	β	τ_R	τ (experimental)[b]
Tm^{3+}:			
$^1D_2 \rightarrow$		72 μs	74 μs
$^3H_4$	0.14		
$^3F_4$	0.44		
$^3H_6$	0.42		
$^1G_4 \rightarrow$		649 μs	480 μs
$^3H_4$	0.17		
$^3F_4$	0.50		
$^3H_6$	0.33		
$^3H_4 \rightarrow$		1.14 ms	1.2 ms
$^3F_4$	0.13		
$^3H_6$	0.87		
$^3F_4 \rightarrow {}^3H_6$	1	9.4 ms	15 ms
Yb^{3+}:			
$^2F_{5/2} \rightarrow {}^2F_{7/2}$	1	1.77 ms	1.8 ms
Nd^{3+}:			
$^4F_{3/2} \rightarrow$		334 μs	400 μs
$^4I_{J=15/2,\ 13/2,\ 11/2,\ 9/2}$	1		

Energy transfer rate parameters (experimental)[c]

Interaction	Process	Rate (s^{-1})	Step
Nd–Yb	b	4×10^6	–
Tm−Yb	d	580	–
Yb−Tm	e	2291	1
Yb−Tm	f	1088	2
Yb−Tm	g	1270	3
Yb−Tm	h	1095	4
Tm−Nd	p	420	–
Tm−Nd	q	6063	–
Tm−Tm	r	~ 0	–
Tm−Tm	s	543	–

[a]Values obtained from the literature (Ref. 15).
[b]Experimental lifetime obtained from best luminescence fitting (in this work).
[c]Experimental transfer rates obtained in this work for Yb(20):Tm(0.5):Nd(1):KY3F.

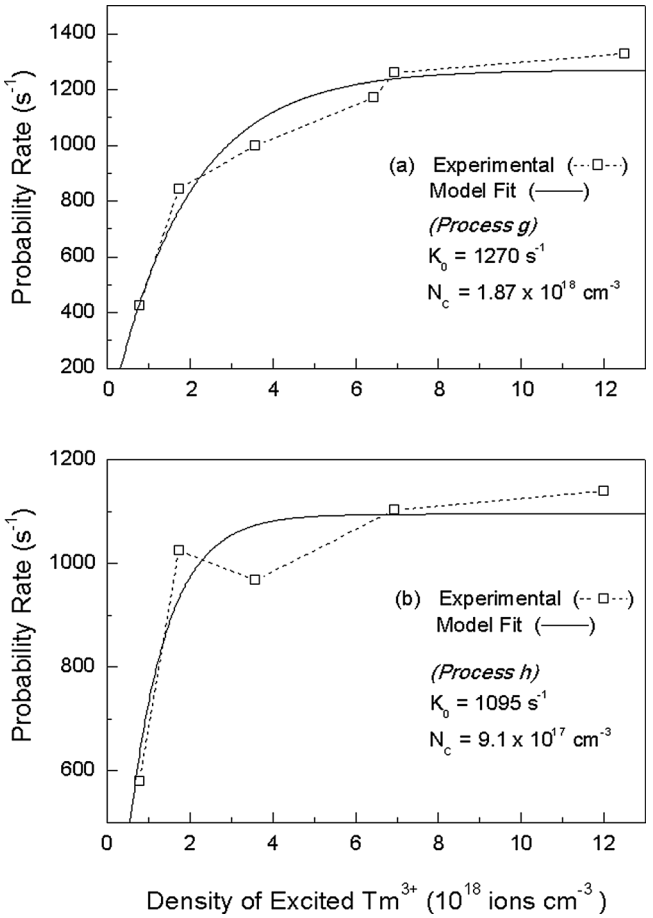

FIG. 8. Rate parameter of $Yb(^2F_{5/2}) \times Tm(^3H_4)$ cross-interaction as a function of the experimental excited Tm^{3+} ion density (N^*) obtained by measuring the luminescence transient of the $^1G_4$ level after (pulsed 4 ns) excitation at 797 nm — that excites also Nd^{3+} ions — shown by (a). (b) Exhibits the results of the probability rate of $Yb(^2F_{5/2}) \times Tm(^1G_4)$ cross interaction as a function of $N^*(Tm^{3+})$ obtained by measuring the luminescence transient of the $^1D_2$ level after excitation (pulsed 4 ns) at 797 nm. Solid lines represent the best fittings using the proposal model for an energy transfer up-conversion involving two ions in the excited state.

large values of N^* should be given by $\eta(N^*) = g/K_0$, where K_0 is the rate parameter constant. The solid line in Fig. 8(a) represents the best fit of g rate probability using the model, which gave $N_C = 1.87 \times 10^{18}$ cm^{-3} and $K_0 = 1270$ s^{-1} (or $W_C = 6.79 \times 10^{-16}$ cm^3 s^{-1} using that $W_C = K_0/N_C$). Solid line in Fig. 8(b) represents the best fit of the rate probability (process h) using the model, which gave $N_C = 9.1 \times 10^{17}$ cm^{-3} and $K_0 = 1095$ s^{-1} (or $W_C = 1.2 \times 10^{-15}$ cm^3 s^{-1}). K_0 values should be used in a rate equation system simulating the operation of a laser because under these circumstances, higher excited Tm^{3+} ion densities ($N^* \geq 10^{19}$ cm^{-3}) are usually present. The proposed model for Yb–Tm transfer (process g and h) predicts a rate linearly dependent on the N^* for $N^* \ll N_C$, i.e., $K_0 \propto N^*$, as has been previously reported for energy transfer up-conversion (ETU) process between two Nd^{3+}ions in the $^4F_{3/2}$ state.[18] Recently it has been demonstrated that ETU rate (s^{-1}) due two Ho^{3+} ions in the $^5I_7$ (or in the $^5I_6$) state of Ho^{3+} in ZBLAN shows a similar dependence on the excitation density of Ho^{3+} ions (cm^{-3}).[19] Detailed investigation of the rate transfer of process f has shown a similar rate transfer behavior exhibited (Fig. 8) for process g. As a consequence, the rate parameter of process f (1088 s^{-1}) determined in Sec. III C must be considered as a rate constant once it was measured using an excitation density $\sim 3 \times 10^{18}$ Tm^{3+} ions cm^{-3}.

IV. DISCUSSION

The energy transfer rate parameters (s^{-1}) involved in the Yb:Tm:Nd system, which were obtained in this work, are given in Table I. Process i could not be observed using direct excitation of Nd^{3+} and Tm^{3+} ions with 797 nm laser excitation because the $^4F_{3/2}$ (Nd^{3+}) excited level rapidly transfer its population to the Yb^{3+} ($\sim$0.25 μs) so triggering process g, i.e., process i will be considered negligible in Yb:Tm:Nd:YLF crystal. All the optical parameters used in the numerical simulation are listed in Table I.

The same methodology applied to Yb(20%):Tm(0.5%):Nd(1%) system to obtain the (Yb × Tm) transfer rate constants of processes e, f, g, and h was employed to the Yb(x):Tm(0.5):Nd(1) systems, where $x = 5$, 10, and 30 mol%. Figure 9 shows the rate constants of (Yb × Tm) cross-interactions as a function of the Yb^{3+} concentration (mol%) in Yb:Tm:Nd:KY3F crystal. Figure 9(a) shows that the rate constant (s^{-1}) of process f exhibits a power law dependence on ytterbium concentration, $K = a(N_{Yb})^b$, where $b = 2.44$ and $a = 0.678$ mol%$^{-1}$. Nevertheless, the transfer rate (K) of processes e, g, and h exhibit a saturation (K_s) that evidences the existence of a critical concentration (N_C) of ytterbium (< 30 mol%) such K must have a ytterbium concentration (N_{Yb}) dependence similarly described by Eq. (4), $K = K_s(1 - \exp(-N_{Yb}/N_C))$, see the results of Fig. 9(b). The following parameters were obtained from best fittings [dashed and solid lines of Fig. 9(b)] using the critical concentration model: (i) (process e) $N_C = 4.3$ mol% and $K_s = 2460$ s^{-1}; (ii) (process g) $N_C = 25.1$ mol% and $K_s = 2065$ s^{-1}, and (iii) (process h) $N_C = 26.3$ mol% and $K_s = 1792$ s^{-1}.

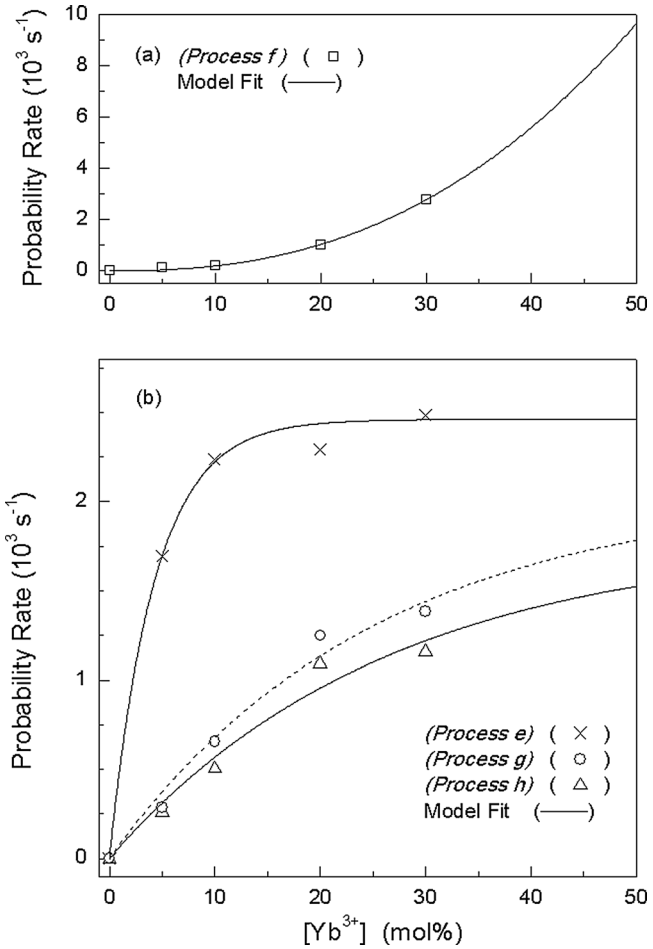

FIG. 9. shows the rate constants of (Yb × Tm) cross-interactions as a function of the Yb^{3+} concentration (mol%) in Yb:Tm:Nd:KY3F crystal. The rate constant (s^{-1}) of process f exhibits a power law dependence on Yb^{3+} concentration with fitting parameters, $b = 2.44$ and $a = 0.678$ mol%$^{-1}$ – see the results in (a). The resting of (Yb × Tm) cross-interactions (processes e, g, and h) exhibit a rate constant saturation value (K_s) with the increasing Yb^{3+} concentration –see the results shown in (b).

A. Rate equations for the (Yb^{3+}, Nd^{3+}), Tm^{3+}-co-doped KY3F system

Figure 3 shows the simplified energy level scheme of Yb:Tm:Nd:KY3F system considered for cw diode laser pumping at 797 nm. n_1, n_2 are the $^2F_{7/2}$ and $^2F_{5/2}$ populations of Yb^{3+} and n_3, n_4, n_5, n_6, and n_7 are the $^3H_6$, $^3F_4$, $^3H_4$, $^1G_4$ and $^1D_2$ populations of Tm^{3+}, and n_8 and n_9 are the $^4I_{9/2}$ and $^4F_{3/2}$ of Nd^{3+}. For Tm^{3+} ion, the $^3F_3$ and the $^3H_5$ excited levels were not considered because they are strongly depopulated by fast multiphonon decay to the next lower lying state. The same argument was used to neglect the $^4I_{11/2}$, $^4I_{13/2}$, $^4I_{15/2}$ and $^4F_{5/2}$ excited levels of Nd^{3+} in the rate equations. The rate equations comprising the model using the fact that $n_1 + n_2 = x/100$ for an Yb^{3+} concentration of x mol% and $n_3 + n_4 + n_5 + n_6 + n_7 = 0.005$ for a Tm^{3+} concentration of 0.5 mol% and $n_8 + n_9 = 0.01$ for an Nd^{3+} concentration of 1 mol% are

$$\frac{dn_1}{dt} = \frac{n_2}{\tau_2} + gn_2n_5 + en_2n_3 - dn_1n_5 + fn_2n_4 - bn_1n_9 + hn_2n_6, \quad (5)$$

$$\frac{dn_2}{dt} = -\frac{n_2}{\tau_2} + dn_1n_5 - gn_2n_5 - en_2n_3 - fn_2n_4 + bn_1n_9 - hn_2n_6, \quad (6)$$

$$\frac{dn_3}{dt} = -\sigma_{35}n_3\frac{I_P}{h\nu} + \frac{n_4}{\tau_4} + \frac{\beta_{53}}{\tau_{R5}}n_5 + \frac{\beta_{63}}{\tau_{R6}}n_6 + dn_1n_5 - en_2n_3 + pn_4n_8 + qn_5n_8 - rn_3n_5 - sn_3n_6 + \frac{\beta_{73}}{\tau_{R7}}n_7, \quad (7)$$

$$\frac{dn_4}{dt} = -\frac{n_4}{\tau_4} + \frac{\beta_{54}}{\tau_{R5}}n_5 + \frac{\beta_{64}}{\tau_{R6}}n_6 - fn_2n_4 + en_2n_3 - pn_4n_8 + 2rn_3n_5 + sn_3n_6 + \frac{\beta_{74}}{\tau_{R7}}n_7 \quad (8)$$

$$\frac{dn_5}{dt} = \sigma_{35}n_3\frac{I_P}{h\nu} - \frac{n_5}{\tau_5} + \frac{\beta_{65}}{\tau_{R6}}n_6 - dn_1n_5 - gn_2n_5 + fn_2n_4 - rn_3n_5 + \frac{\beta_{75}}{\tau_{R7}}n_7 + sn_3n_6 - qn_5n_8, \quad (9)$$

$$\frac{dn_6}{dt} = -\frac{n_6}{\tau_6} + gn_2n_5 - hn_2n_6 - sn_3n_6, \quad (10)$$

$$\frac{dn_7}{dt} = -\frac{n_7}{\tau_7} + hn_2n_6, \quad (11)$$

$$\frac{dn_8}{dt} = -\sigma_{89}\frac{I_P}{h\nu}n_8 + \frac{n_9}{\tau_9} + bn_1n_9 - pn_4n_8 - qn_5n_8, \quad (12)$$

$$\frac{dn_9}{dt} = \sigma_{89}\frac{I_P}{h\nu}n_8 - \frac{n_9}{\tau_9} - bn_1n_9 + pn_4n_8 + qn_5n_8, \quad (13)$$

where I_P is the pump intensity given in W cm^{-2} and $h\nu$ is the photon energy at 797 nm. β_{ij} represents the luminescence branching ratio and τ_{Ri} is the radiative lifetime of excited states of Tm^{3+} labeled as $i = 4$, 5, 6 and 7.

B. Numerical simulation of the rate equation system

Calculations were performed for the Yb(x):Tm(0.5):Nd(1):KY3F and Yb(x):Tm(0.5):KY3F systems ($x = 5$, 10, 20, and 30%) using a computer program developed in Scilab language, incorporating the Runge-Kutta numerical method. Figure 10 shows the time evolutions of $n_3(t)$ and $n_6(t)$ and Δn, the population inversion $n_6(t) - B_i\, n_3(t)$ of Tm^{3+} after switching the pump laser at $t = 0$ (using a pump rate of 560 s^{-1} at 797 nm B_i is the Boltzmann occupation factor of ground state sublevels). Equilibrium in the populations was obtained after 3 ms in Yb(30%):Tm(0.5%):Nd(1%):KY3F system, see Figs. 10(b) and 10(c) for n_6 and n_3 normalized populations, respectively. At that stage, the value of Δn was obtained. With the purposes of verifying how the $^3H_6$ multiplet splitting will affect the calculated population inversion we sketched out the following arguments. The $^3H_6$ ground state of Tm^{3+} has eight sublevels localized at 0 (1), 357 (2), 365 (3), 416 (4), 426 (5), 444 (6), 471 (7), and 480 (8) cm^{-1} (Ref. 15) having Boltzmann occupation factors (B_i) equal to 0.6550, 0.1114, 0.0536, 0.0395, 0.0396, 0.0363, 0.0317, and 0.0314, respectively calculated using $T = 300$ K (room temperature). For the purposes of calculating the population inversion, the $^1G_4$ multiplet is located at 21180 cm^{-1} with a Boltzmann occupation factor $B = 1$. Eight emission lines are expected at 472.1 (1), 480.2 (2), 480.4 (3), 481.6 (4), 481.8 (5), 482.3 (6), 482.9 (7), and 483.1 nm (8). The population inversion for each $^1G_4 \rightarrow {}^3H_6$ (i) transition will be given by $\Delta n_i = n_6(t) - B_i\, n_3(t)$. We have seen that $\Delta n > 0$ for all the emission lines (2 –8). Figure 11 shows the results obtained by the numerical simulation for cw 797 nm laser pumping. Figure 11 shows the population inversion for the emission lines from $^1G_4 \rightarrow {}^3H_6$ transition as a function of the pumping rate for two systems: Yb(20%):Tm(0.5):Nd(1):YLF (a) and Yb(30%):Tm(0.5):Nd(1):KY3F (b) for comparison. It is observed that the emission line (8) at 483.1 nm of Tm^{3+} in KY3F has the highest population inversion effect and exhibits the lowest pumping rate threshold of ~98 s^{-1} that is equivalent to the pumping intensity of 3.3 KW cm^{-2} for Yb-doped (30%) KY3F—see Fig. 11(b). It is observed that Yb-doped (20%) YLF has smaller pumping rate threshold (60 s^{-1} or 2 KW cm^{-2}) for the emission line (10) at 481.4 nm in comparison with KY3F. It was observed that a population inversion of $^1D_2 \rightarrow {}^3F_4$ emission line at 456.2 nm starts only for high Yb doping (50 mol%) in KY3F with a threshold

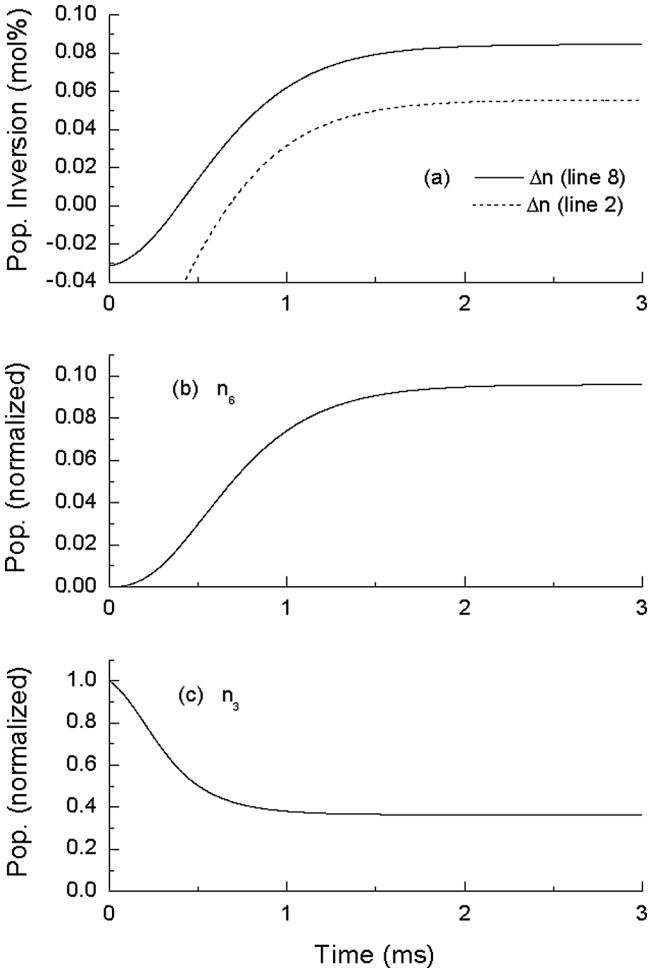

FIG. 10. Calculated evolution of the excited state populations (normalized) of Tm^{3+} obtained by numerical simulation of the rate equations for Yb(30):Tm(0.5):Nd(1):KY3F crystal. The simulations were obtained under a continuous pump rate of 560 s^{-1} at 797 nm. Normalized populations $n_6(t)$ and $n_3(t)$ are shown in Fig. 10(a) and 10(c), respectively. Population inversion was obtained for the laser lines (2 – 8). Gain for the laser lines [(2) and (8)] that emit at 480.2 and 483.1 nm are shown by the dashed and solid lines of Fig. 10(a).

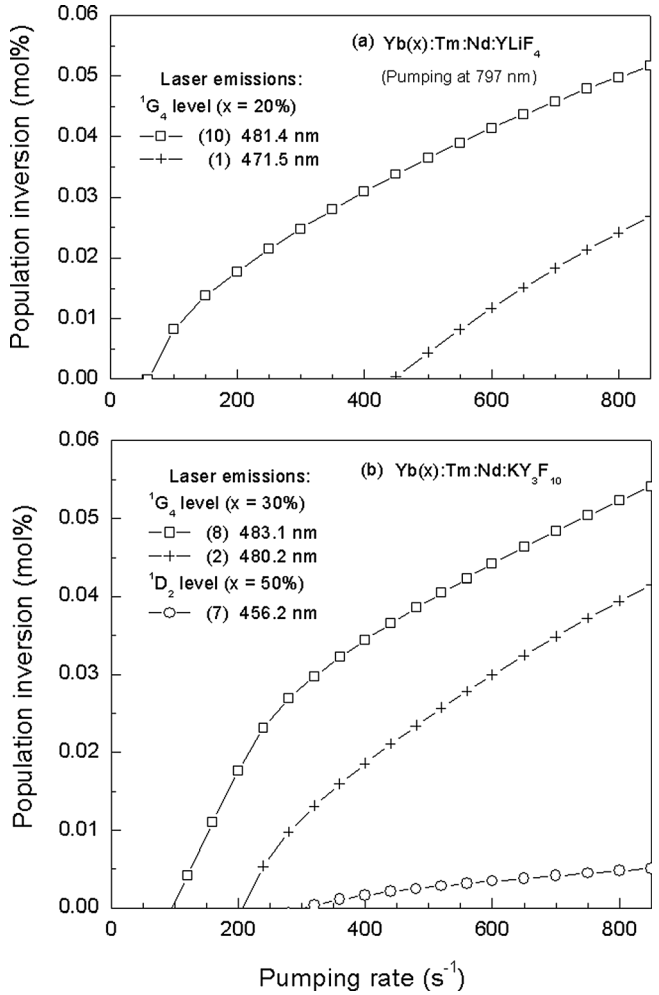

FIG. 11. Results of the population inversions (in mol%) obtained for the emission lines at 480.2 nm (2) and 483.1 nm (8) involved in the $^1G_4 \rightarrow {}^3H_6$ transition of Tm^{3+} are shown in (b) for Yb(30):Tm(0.5):Nd(1):KY3F. Results were obtained by numerical simulation for a continuous laser pumping at 797 nm. (a) Exhibits the results for the emission lines at 471.5 nm (1) and 481.4 nm (10) obtained for the case of Yb(20):Tm(0.5):Nd(1):YLF crystal for comparison.

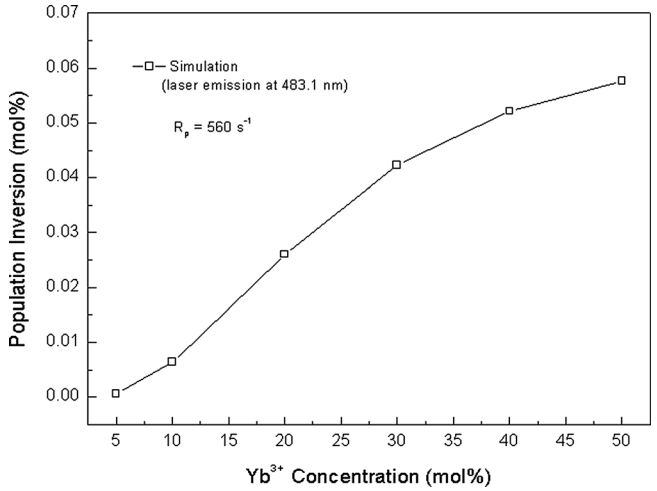

FIG. 12. Shows the population inversion (Δn) for the emission line at 483.1 (8) obtained by numerical simulation for a cw laser pumping at 797 nm with a pumping rate constant equal to 560 s^{-1} for the Yb(x):Tm(0.5):Nd(1):KY3F crystal. A maximization of Δn is obtained for Yb^{3+} concentration between 40 and 50 mol%.

pumping rate of ~304 s^{-1} or 10.3 KW cm^{-2}-see the results showed in Fig. 11(b).

We have observed also none population inversion for the $^1G_4 \rightarrow {}^3H_6$ transition of Tm^{3+} in Yb(x):Tm:KY3F, where $x = 5$, 10, 20, and 30 mol%, when setting Nd^{3+} concentration to zero in the numerical simulation for cw 797 nm pumping, similar to observed for Yb:Tm:YLF crystal. The results presented in Fig. 11 show that 1 mol% of Nd^{3+} ions leads to a positive Δn values with a threshold pumping rate of ~98 s^{-1} calculated for the laser emission at 483.1 nm in KY3F system. The pumping rates can be converted to pump intensities I_P (W cm^{-2}) using $I_P = R_P\ (h\nu)/\sigma_{abs}$, where $\sigma_{abs}({}^3H_6 \rightarrow {}^3H_4) = 7.2 \times 10^{-21}$ cm^2 at 797 nm for Tm^{3+} in KY3F crystal.

However, we have used the extrapolated values of rate constants of processes *e, f, g,* and *h* from curves exhibited in Fig. 9, in order to get the best Yb concentration that can maximize the laser emission at 481.3 nm (line 8) in Yb:Tm:Nd:KY3F pumped by cw laser at 797 nm with a constant pumping rate of 560 s^{-1}. Figure 12 shows that maximization occurs for an Yb concentration between 40 and 50 mol%.

We have observed also a negative Δn values obtained by using the numerical solutions of the rate equations [Eqs. (5)–(13)] applied to the Yb(x):Tm(0.5):KY3F ($x = 5$, 10, 20, and 30%) under cw pumping at 960 nm. In this case, negative values of population inversion were obtained for most of all the laser emissions involved in the $^1G_4 \rightarrow {}^3H_6$ transition.

V. CONCLUSIONS

Studying the optical properties of KY3F doped with Yb/Tm/Nd it can be concluded that the crystal is efficient and generates blue emission by two-photon process arising from 797 nm excitation, which excites simultaneously Tm^{3+} and Nd^{3+}. A full efficient energy transfer from Nd^{3+} ($^4F_{3/2}$) to Yb^{3+} ($^2F_{5/2}$) was noticed considering that the Nd^{3+} emission from $^4F_{3/2}$ is very shortened exhibiting a lifetime of 0.25 μs. The cross-relaxation $Yb(^2F_{5/2}) \times Tm(^3H_4)$ leads to the $^1G_4$ population grown by two order process (or two-photon), while in the case of Yb(20):Tm system, a $Tm(^3H_4) \rightarrow Yb(^2F_{7/2})$ energy transfer is required first to excite an Yb^{3+} ion with a transfer rate constant of 580 s^{-1}. This Tm → Yb transfer (or excitation) rate is much smaller than the Nd → Yb transfer rate of 4×10^6 s^{-1} observed in the case of Nd-doped (1 mol%) Yb(x):Tm:KY3F ($x = 10$, 20, and 30%).

With all the relevant energy transfer rate parameters measured available, we numerically solved the rate equations for the Yb:Tm:Nd:KY3F and Yb:Tm:KY3F systems under cw laser pumping at 797 nm. The results established that Yb(20−30 mol%):Tm (0.5 mol%)-doped KY3F crystal that was co-doped with 1 mol% of Nd^{3+} showed considerable improvement in the value of Δn as compared to the corresponding Yb:Tm-doped

KY3F crystal because of strong and fast $Nd \rightarrow Yb$ transfer ($\tau \sim 0.25\ \mu s$) followed by $Yb(^2F_{5/2}) \times Tm(^3H_4)$ cross relaxation that efficiently populates the upper laser level ($^1G_4$). A threshold pumping rate of 98 s^{-1} was obtained for 481.3 nm emission line of Yb(30):Tm(0.5): Nd(1):KY3F to provide population inversion, $\Delta n > 0$. Considering the population distribution of Stark levels of $^3H_6$ state of Tm^{3+} the relative gain of each emission line (1 – 8) was estimated by means of looking its Δn_i value. Because it is observed that $\Delta n_i > 0$ for the emission lines $i = 2$ to 8 we claim that Yb(x):Tm(0.5):Nd(1):KY3F crystal where $x = 20 - 50\%$ is suitable for obtaining laser action near 480 nm under cw pumping at 797 nm. It was also seen that the Nd^{3+} doping of 1 mol% is decisive to have gain for blue emission, since the gain become negative in Yb:Tm system according to the numerical simulation results. Results of numerical simulation showed that Yb(x):Tm(0.5):KY3F ($x = 5$, 10, 20, and 30%) does not have population inversion for the $^1G_4 \rightarrow {}^3H_6$ transition, when pumped by 960 nm cw laser. We have observed also that the $^1D_2$ excited Tm^{3+} level has potential gain only for the laser emission at 453.1 for high Yb-doped (50 mol%) in Yb:Tm:Nd:KY3F crystal pumped by 797 nm cw laser.

The numeric method employed in this work to investigate the small signal gain of blue laser emission (~480 nm) of Tm^{3+}-doped KY3F crystal has been previously applied to describe the laser performance at 2.97 μm of Ho^{3+}:ZBLAN and Ho^{3+}:Pr^{3+}:ZBLAN glass optical fiber lasers (cw) pumped by 1000 nm (Yb-optical fiber laser) and 650 nm (diode laser), respectively, with success.[19,20] It constitutes a useful tool of analyzing the potential laser gain of laser materials and the dopants (activator or sensitizer) concentration optimization.

ACKNOWLEDGMENTS

The authors thank financial support from FAPESP (Grants Nos. 1995/4166-0 and 2000/10986-0) and CNPq.

[1]Y. L. Tang, Y. Yang, X. J. Cheng, and J. Q. Xu, Chinese Opt. Lett. **6**, 44 (2008).
[2]M. K. Tollefson, M. T. Gettman, and I. Frank, J. Urol. **179**, 365 (2008).
[3]K. Scholle, E. Heumann, and G. Huber, Laser Phys. Lett. **1**, 285 (2004).
[4]Y. Kishi and S. Tanabe, J. Am. Ceram. Soc. **89**, 236 (2006).
[5]L. Tsonev, Opt. Mater. **30**, 892 (2008).
[6]R. P. Rao, J. Lumin. **113**, 271 (2005).
[7]K. Miura, H. Kawamoto, Y. Kubota, N. Nishimura, and Y. Kita, Japan patents GB2302442-A (15 Jan 1997), GB2302442-B (22 Sep 1999), FR2735288-A1 (13 Dec 1996), US5684815-A (04 Nov 1997) (Central Glass Co. Ltd.).
[8]N. P. Barnes, IEEE J. Sel. Top. Quantum Electron. **13**, 435 (2007).
[9]E. Boulma, M. Diaf, J. P. Jouart, M. Bouffard, J. L. Doualan, and R. Moncorge, J. Phys.:Condens. Matter **18**, 6721 (2006).
[10]E. Boulma, M. Diaf, J. P. Jouart, M. Bouffard, J. L. Doualan, and R. Moncorge, Opt. Mater. **30**, 1028 (2008).
[11]M. Ito, S. Hraiech, C. Goutaudier, K. Lebbou, and G. Boulon. J. Cryst. Growth **310**, 140 (2008).
[12]K. J. Kim, A. Jouini, A. Yoshikawa, R. Simura, G. Boulon, and T. Fukuda, J. Cryst. Growth **299**, 171 (2007).
[13]I. M. Ranieri, L. C. Courrol, A. F. Carvalho, L. Gomes, and S. L. Baldochi, J. Mater Sci. **42**, 2309 (2007).
[14]L. D. da Vila, L. Gomes, L. V. G. Tarelho, S. J. L. Ribeiro, and Y. Messaddeq, J. Appl. Phys. **93**, 3873 (2003).
[15]M. Diaf, A. Braud, C. Labbé, J. L. Doualan, S. Girard, J. Margerie, R. Moncorgé, and M. Thuau, Can. J. Phys. **77**, 693 (1999).
[16]L. Gomes and F. Luty, Phys. Rev. B **30**, 7194 (1984).
[17]A. F. H. Librantz, L. Gomes, L. C. Courrol, I. M. Ranieri, and S. L. Baldochi, J. Appl. Phys. **105**, 113503 (2009).
[18]J. Fernandez, R. Balda, M. L. M. Lacha, A. Olega, and J. L. Adam, J. Lumin. **94**, 325 (2001).
[19]A. F. H. Librantz, S. D. Jackson, F. H. Jagosich, L. Gomes, G. Poirier, S. J. L. Ribeiro, and Y. Messaddeq, J. Appl. Phys. **101**, 123111 (2007).
[20]A. F. H. Librantz, S. D. Jackson, L. Gomes, S. J. L. Ribeiro, and Y. Messaddeq, J. Appl. Phys. **103**, 023105 (2008).